Molecular Genetics and Metabolism 145 (2025) 109149

Contents lists available at ScienceDirect

Molecular Genetics and Metabolism

journal homepage: www.elsevier.com/locate/ymgme

Research Paper

Biochemical investigation of pathogenic missense mutations of human 4-amino butyrate aminotransferase towards the understanding of the molecular pathogenesis of GABA transaminase deficiency.

Giulia Ambrosini [1], Fulvio Floriani [1], Vittoria Manni, Ilaria Dando, Riccardo Montioli [*]

Department of Neurosciences, Biomedicine and Movement Sciences, Section of Biological Chemistry, University of Verona, 37134 Verona, Italy

ARTICLE INFO

Keywords:
4-Amino butyrate aminotransferase
GABA-AT
GABA transaminase deficiency
Pathogenic variants
Missense mutations

ABSTRACT

Gamma-amino butyrate aminotransferase (GABA-AT or ABAT) is a pyridoxal 5′-phosphate (PLP)-dependent enzyme that catalyzes the conversion of GABA and α-ketoglutarate into succinic semialdehyde and L-glutamate. In humans, the primary physiological role of GABA-AT is to control the level of GABA in neuronal tissues. Mutations on *ABAT* gene are associated to GABA-AT deficiency, an ultra-rare autosomal recessive disorder characterized by accelerated linear growth, severe psychomotor retardation, seizures, hypotonia, and hyperreflexia. So far, several missense pathogenic mutations of GABA-AT have been identified; however, their molecular effects at protein level have been poorly investigated. In this work a biochemical characterization of 10 pathogenic variants of human GABA-AT was carried out by expressing the protein in HEK-293 cells. Moreover, *in-silico* analyses of the variants were performed to corroborate the experimental findings. Altogether, the data obtained on protein expression level, GABA transaminase activity, and the predicted structural impact allowed us to classify the variants into three distinct groups, such as: (i) variants with strong structural and catalytic defects (p.P152S, p.L211F, and p.L478P); (ii) variants characterized mainly by a strong catalytic defect (p.R220K, p.Q296H, and p.R377W); (iii) variants exhibiting moderate structural and catalytic defects maintaining substantial transaminase activity (p.R92Q, p.F213C, p.G465D, and p.G465R). Based on these results, we provide a picture of the molecular defects of different GABA-AT pathogenic variants with the aim of gaining insights into the enzymatic phenotypes in GABA-AT deficiency.

1. Introduction

The γ-Amino butyrate aminotransferase (GABA Transaminase, GABA-AT, E.C. 2.6.1.19) is a pyridoxal 5′-phosphate (PLP)-dependent enzyme that catalyzes the transfer of the amino group of GABA to α-ketoglutarate (α-KG), producing succinic semialdehyde and L-glutamate. This enzyme belongs to a large family of homologous aminotransferases that operate by the "ping-pong" mechanism consisting of two coupled half-reactions in which the PLP cofactor shuttles between its pyridoxal and pyridoxamine forms [1]. The enzyme, encoded by the *ABAT* gene (NM_020686.6) on chromosome 16p13, is equipped with a mitochondrial targeting sequence (MTS) of 29 aa required for its localization in the mitochondrial matrix. Together with glutamate decarboxylase, GABA-AT transaminase controls the concentration of GABA in the brain, an important neurotransmitter involved in the regulation of brain neuronal activity. A second role of GABA-AT in the mitochondrial nucleoside salvage pathway has also been suggested [2]. The crystal structure of pig liver GABA-AT (96 % identity with human GABA-AT) has been firstly determined alone, or in complex with vigabatrin (an antiepilepsy drug), or with the close analogue γ-ethynyl-GABA to 3.0 Å [3,4]. GABA-AT has a dimeric structure composed of identical monomers tightly intertwined. The two PLP cofactors forming a Schiff base with Lys329 are located close to the subunit interface. Each monomer comprises a large domain (residues 81–375) forming most of

Abbreviations: PLP, pyridoxal-5′-phosphate; GABA, 4-Amino butyrate; hGABA-AT, human GABA aminotransferase; αKG, α-ketoglutarate; SSA, succinic semialdehyde; HEK, human embryonic kidney; SSADH, succinic semialdehyde dehydrogenase; WB, western blotting; WT, wild type..

* Correspondence to: Riccardo Montioli, Department of Neurosciences, Biomedicine and Movement Sciences, Section of Biological Chemistry, University of Verona, Strada Le Grazie 8, 37134 Verona, Italy.

E-mail address: riccardo.montioli@univr.it (R. Montioli).

[1] Equal contribution

https://doi.org/10.1016/j.ymgme.2025.109149
Received 24 April 2025; Received in revised form 19 May 2025; Accepted 20 May 2025
Available online 21 May 2025

the subunit interface, an N-terminal domain (residues 11–71), and a C-terminal domain (residues 376–472).

Abnormal low levels of GABA in the brain are associated with severe neurological disorders, such as epilepsy, Huntington disease, Parkinson's disease, and Alzheimer's disease [5–8]. High levels of GABA are associated with the inherited disorders of GABA catabolism GABA-AT deficiency (OMIM 613163) and succinic semialdehyde (SSADH) deficiency (OMIM 271980), which, differently from GABA-AT deficiency, presents, as a hallmark, high levels of γ-hydroxybutyrate (GHB) [9]. The GABA-AT deficiency is an ultrarare disease reported and characterized in only few patients [10–16], and it is caused by mutations in the *ABAT* gene. The exiguous reports suggest it seems to be much rarer than other disorders of GABA metabolism [17]. This disorder is characterized by high levels of GABA in cerebrospinal fluid (CSF), plasma, and urine. Clinical manifestations include accelerated linear growth, severe psychomotor retardation, convulsion, hypotonia, and hyperreflexia [10]. The disease has a broad phenotypic spectrum with variable response to treatments [15].

At present, the HGMD database (https://www.hgmd.cf.ac.uk/ac/index.php) (accessed on Nov, 11th 2024) reports 8 missense pathogenic mutations of the *ABAT* gene associated with GABA-AT deficiency. Such mutations generate the GABA-AT pathogenic variants p.R92Q [12], p.P152S [13], p.L211F [13], p.R220K [11], p.Q296H [14], p.R377W [15], p.G465R [13], and p.L478P [12]. In addition, the pathogenic variants p.F213C and p.G465D have been reported [16]. At the protein level, little is known about the phenotype of the human GABA-AT (hGABA-AT) variants. Here we present a biochemical characterization of 10 pathogenic variants of the hGABA-AT. Analyses were performed by expressing the wild-type form or the hGABA-AT variants in HEK-293 cells. Moreover, bioinformatics analyses were also performed to corroborate the experimental results. The data obtained allowed us to classify the mutants based on their soluble expression level and their catalytic activity, with the aim of acquiring information about the molecular defect of each pathogenic hGABA-AT variant.

2. Materials and methods

2.1. Drugs and chemicals

4-amino butyrate (GABA), α-ketoglutarate (α-KG), pyridossal-5′-phosphate (PLP), NADH, protease inhibitor cocktail EDTA-free, isopropyl-D-thiogalactoside, Hepes and imidazole were purchased from Merck & Co (Rahway, NJ, USA). All other chemicals were of the highest purity available.

2.2. Cloning and site-directed mutagenesis

His-tagged succinic semialdehyde dehydrogenase from *E. coli* (His-SSADHe) coding sequence synthetized by Eurofins Genomics s.r.l. (Ebersberg, Germany) was amplified from the synthesis vector with the 5' GACTCATATGCATCACCACCATCATCATACCATTAC 3′ forward primer and 5' CAGTAAGCTTTCAGATCCGGTCTTTCCACACC 3′ reverse primer to add the restriction sites *Nde*I and *Eco*RI. The expression plasmid was obtained by cloning the amplified sequence in pET43a expression vector by means of the same restriction sites. The coding sequence of the full-length isoform 1 of the human 4-aminobutyrate aminotransferase synthetized by Eurofins Genomics was amplified from the synthesis vector with the forward primer 5' GATCAAGCTTATGGCCTCCATGTTGCTCGCC 3′ and the reverse primer 5' GTACCTCGAGTCACTTGAAGTCTGCTAAGATGTCACTG 3′ to add the restriction sites *Hin*dIII and *Xho*I. The human GABA-AT complete ORF was then cloned into pcDNA3.1 vector, by means of the HindIII and XhoI restriction enzymes, obtaining the pGABA-AT expression vector.

The hGABA-AT amino acid substitutions p.R92Q, p.P152S, p.L211F, p.F213C, p.R220K, p.Q296H, p.R377W, p.G465D, p.G465R, and p.L478P were introduced by site-directed mutagenesis using the QuickChange II kit (Agilent Technologies, Santa Clara, CA, US) using the pGABA-AT as the template and the mutagenetic primers listed in **Table S1**. The sequences of the His-SSADHe and all the hGABA-AT expressing constructs were confirmed by DNA sequence analysis of the whole coding regions.

2.3. Cell lines

All the cell lines used in this paper, *i.e.*, SH-SY5Y (a human neuronal cell line), HEK-293 (a human embryonic kidney cell line), HaCaT (a human keratinocytes cell line), HPDE-1 (a human pancreatic duct epithelial cell line), and fibroblasts were grown in RPMI-1640 supplemented with 10 % FBS and 50 μg/mL gentamicin sulfate (all from Gibco/Life Technologies, USA), and cells were maintained at 37 °C with 5 % CO_2. In all the assays, cells were cultured in proliferating conditions and not in cell growth arrest due to contact inhibition. Cell pellets were lysed in lysis buffer [*i.e.*, 1 mM Na_3VO_4, 1 mM NaF, 2.5 mM EDTA, 1 mM phenylmethylsulfonyl fluoride (PMSF), 12 mM NaCl, 1× complete protease inhibitor cocktail, and RIPA buffer pH 8.0 (150 mM NaCl, 50 mM Tris-HCl, 1 % Igepal, 0.5 % sodium deoxycholate, and 0.1 % SDS)], by 30 min incubation in ice; this procedure was able to disrupt organelles completely, thus allowing to extract also mitochondrial GABA-AT. The whole cell extract was separated by centrifugation (13,000 *g* for 10 min, 4 °C) to obtain the soluble fraction. Protein concentration of the soluble cell lysate was determined in duplicate by using the Bradford protein assay and detecting absorbance (595 nm) with Tecan Infinite 200 PRO multiplate reader.

2.4. Transient transfection of GABA-AT variants

HEK-293 were transfected using the DreamFect Gold (OZBiosciences, Marseille, FR) according to the manufacturer's instructions. Briefly, 3×10^5 cells were seeded in 6-well plates and incubated at 37 °C, 5 % CO_2 one day before the transfection. All plasmid DNA solutions used were brought to the same concentration for the preparation of DNA: transfection reagent mix. Following the addition of transfection complexes, cells were incubated for 72 h before collection.

2.5. Western-blotting analysis

From 10 to 40 micrograms of soluble wild-type or mutants cell lysates, respectively, were loaded per lane on a 12 % SDS-PAGE gel along with the PageRuler™ Prestained Protein Ladder (ThermoFisher Scientific, Waltham Massachusetts, US) molecular mass marker. Proteins were then transferred on a PVDF membrane using the Mini Trans-Blot® Cell and Criterion™ Blotter (Bio-Rad) followed by blocking on 5 % milk (*w/v*) in TBST buffer (10 mM Tris-HCl pH 7.2, 0.1 M NaCl and 1 % Tween20), at 37 °C for one hour. For GABA-AT detection, the membrane was incubated with the primary antibodies at an appropriate dilution in blocking solution overnight at 4 °C. Primary antibodies included: GABA-AT (dilution 1:1000, Origene Rockville US), TOMM20 (1:1000, Cell Signaling Technology, Danvers, MA, USA), and Vinculin (1:1000, Cell Signaling Technology). Peroxidase-conjugated anti-mouse IgG was used as secondary antibody (dilution 1:8000). Band detection was performed by using the enhanced chemiluminescence (ECL) substrate reagent using the ChemiDoc MP Imaging System (Bio-Rad Laboratories, Hercules, CA, USA). Band volume (intensity/mm^2) was quantified using the software ImageJ (NIH Image, Bethesda, MD, USA). Amido black staining was used to confirm loading in different lanes.

2.6. Immunofluorescence microscopy

GABA-AT subcellular localization was investigated by confocal microscopy experiments performed in fixed cells. Approximately 5×10^4 cells were seeded into each well of a 24-well plate, containing a 13-mm glass coverslip and, 24 h later, were transfected with specific pcDNA.

After 72 h cells were fixed in 4 % (*w/v*) paraformaldehyde, permeabilized with 0.05 % Triton X-100 in PBS and blocked in 5 % BSA in PBS. For the immunolabelling, mouse monoclonal anti-human GABA-AT and anti-TOMM20 from rabbit (to stain mitochondria, Life Technologies) were used as primary antibodies, and Alexa Fluor conjugated antibodies (AF488 and AF568, Life Technologies) were used as secondary antibodies; nuclei were stained with DAPI (Molecular Probes). The coverslips were then mounted over slides in AF1 medium (Dako). Images were captured using a confocal laser-scanning fluorescence microscope Leica SP5 (Molecular Probes, Leica Microsystem, Manheim, Germany) at 63× magnification. Three-dimensional stack images of cells were deconvolved using Huygens Professional software package (version 19.04, Scientific Volume Imaging B.V. Hilversum The Netherlands, http://svi.nl, accessed on 1st January 2021). For qualitative analysis, the ImageJ software was used (NIH Image, Bethesda, MD, USA). Figure cropping and labelling were performed using Adobe Photoshop.

2.7. Isolation of mitochondria

Mitochondria were isolated according to a specific protocol perfected in our laboratory. Specifically, cell pellets were resuspended and homogenized with a reserved mortar in an extraction buffer (0.25 M sucrose, 20 mM HEPES pH 7.5, 10 mM KCl, 1.5 mM $MgCl_2$, 1 mM EDTA, 1 mM EGTA, 1 mM DTT, 0.1 mM PMSF, 1× proteases inhibitors cocktail) and then incubated on ice for 30 min. After incubation, samples were centrifuged at 800 *g* for 10 min at 4 °C, and then the supernatants were centrifuged at 11,000 *g* for 15 min at 4 °C to separate the cytosolic fraction. The pellets were washed several times with the extraction buffer and finally resuspended in the mitochondrial buffer (50 mM Tris-HCl pH 6.8, 1 mM EDTA, 0.5 % TritonX-100, 1× proteases inhibitors cocktail).

2.8. Expression and purification of His-SSADHe

The *E. coli* BL21 (DE3) cells transformed with the His-succinate dehydrogenase (His-SSADHe) expressing plasmid were grown in shaking condition at 37 °C in 1.5 L of Luria-Bertani broth medium to reach an optical density at a wavelength of 600 nm of 0.6–0.8. The expression was induced with 0.2 mM IPTG for 15 h at 30 °C. Cells were harvested and resuspended in 20 mM sodium phosphate, 0.5 M sodium chloride and 20 mM imidazole pH 7.4 (buffer A), 0.5 mM PMSF and protease inhibitor EDTA-free cocktail (Sigma). Lysozyme was added to a final concentration of 0.2 mg/mL and incubated 20 min at room temperature. After a freeze-thaw, cells were sonicated for 5 min through a Benchmark Pulse 150™ Ultrasonic Homogenizer in ice (2″ pulse, 3″ pause) and centrifuged at 16,000 *g* for 30 min at 4 °C. The supernatant was then loaded on a HisTrap HP 5 mL column equilibrated with buffer A. By using the buffer B (20 mM sodium phosphate and 0.5 M sodium chloride, 500 mM imidazole pH 7.4), a linear gradient of 60 mL from 20 to 500 mM imidazole was applied. Active fractions were then pooled and concentrated using an Amicon Ultra 15 unit (Millipore), diluted in 50 mM HEPES, 150 mM NaCl pH 8.0 and then concentrated again. Purified and buffer-exchanged protein was stored at −80 °C.

2.9. GABA-AT catalytic activity assays

GABA transaminase activity was measured by a spectrophotometric couple assay with the recombinant His-SSADHe. The soluble fraction of the transfected HEK-293 cells (50 μg-200μg) was tested for the GABA transaminase activity in 50 mM HEPES, 150 mM NaCl pH 8, in the presence of 50 μM NAD^+, 10 μM recombinant His-SSADHe, 30 mM GABA, 50 mM α-KG and 30 μM PLP. The time course of the NADH synthesis was monitored at 340 nm at 25 °C using a JASCO V-550 spectrophotometer.

2.10. In silico analyses

The coordinate file of the structure of GABA aminotransferase from *sus scrofa* available on Protein Data Bank (pdb file 1ohv) was used to determine the amino acids conservation score and to generate the coordinate file of the GABA-AT dimer for the calculation of ΔΔG values and the *in silico* mutagenesis. The conservation analysis was performed by the Consurf Server (https://consurf.tau.ac.il/, accessed on 07th February 2025), using the HMMR as the homolog search algorithm between 35 % and 95 % of homology, the UniProt database, and CLUSTALW alignment software. The amino acid conservation score was expressed on a scale of 1 (not conserved) to 9 (highly conserved). The ΔΔG value for each mutation was predicted starting from the dimeric unit structure of *sus scrofa* GABA transaminase using three different tools, mCSM server [18], DUET server [19] and Dynamut 2 server [20]. The *in silico* mutagenesis followed by energy minimization process was performed by Maestro software v14.3 (Schrödinger, New York, NY, USA). The energy minimization process was carried out before and after the mutagenesis on the GABA-AT structure by using VSGB solvation model, OPLS4 forcefield [21] with RMS gradient for convergence of 0.01 kcal/mol/Å.

2.11. Statistical analysis

Results of western-blotting and catalytic activity results are presented as mean ± standard error of the mean (SEM) of at least three different biological replicates. Statistical differences were determined by Student's *t*-test two-sided. Data were analyzed using GraphPad Prism software (version 7.0) (San Diego, CA, USA) and statistical significance was defined as *p*-values <0.05, 0.01, or 0.001.2.1.

3. Results

3.1. In silico analysis of the mutation sites

The *in silico* analyses were performed starting from the available crystal structure of the *sus scrofa* GABA-AT [3]. Conservation analysis revealed that almost all the mutated residues are highly conserved among 150 homologous proteins and none or few alternative residues have been found at the corresponding positions (**Table S2**). Two exceptions are p.R92Q, and p.L211F which exhibited a lower conservation score mainly due to the presence of alternative residues placed at the corresponding position on the homologous sequences. The ΔΔG values of all the pathogenic variants, calculated by means of three different tools (**Table S3**), suggested that, albeit to a different extent, all the mutations are predicted to have a destabilizing impact on the protein structure. From the inspection of the dimeric unit structure, these 10 mutations cause the substitution of residues spread over the protein's large and C-terminal domains (Fig. 1). The possible local structural effects of the pathogenic substitutions p.R92Q, p.P152S, p.L211F, p.F213C, p.R220K, p.Q296H, p.R377W, p.G465D, p.G465R, and p.L478P were probed by *in silico* mutagenesis analysis (see materials and methods). Arg92 is located on the protein surface far from the active site and interacts with the N-terminal arm. The p.R92Q substitution (**Fig. S1A**) is expected to impair most of the original interactions and to alter the local surface charge. Pro152 belongs to a connection loop of the α-β system of the large domain (**Fig. S1B**). Indeed, the p.P152S missense change introduces a polar residue into a hydrophobic cleft and the Pro replacement is expected to alter the backbone flexibility. Leu211 and Phe213 belong to the same loop 199–222 and are immersed into a hydrophobic environment (**Figs. S1C** and **S1D**). It is noteworthy that the same loop hosts the Phe217, one of the fundamental PLP-bonding residues that engages the pyridine ring through a π-π interaction. The steric hindrance introduced by the p.L211F substitution, or the loss of hydrophobic contacts caused by the p.F213C, might impact the loop199–222 conformation. Arg220 is located at the active site, and it

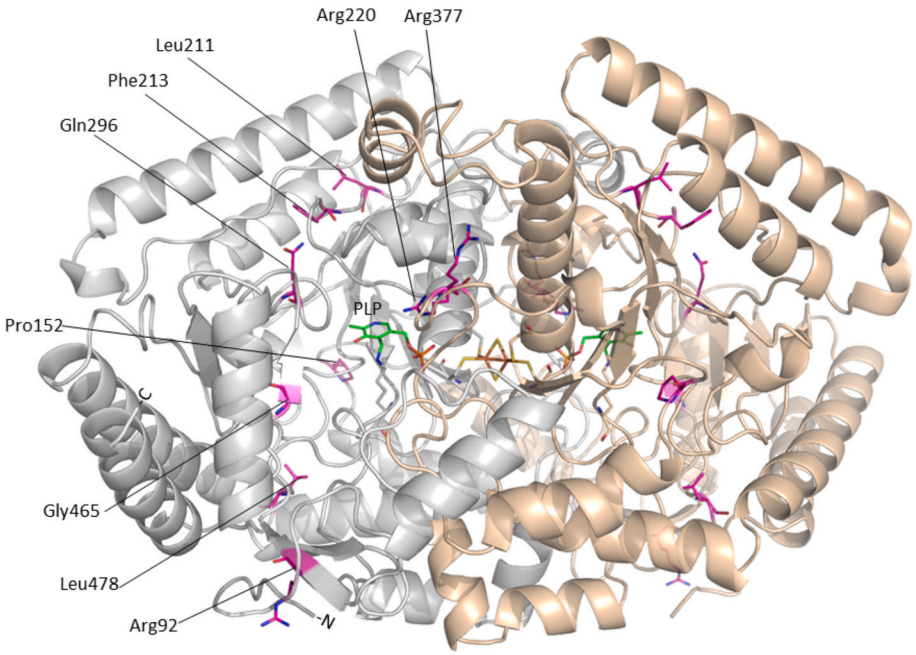

Fig. 1. Structural distribution of the pathogenic amino acid substitution sites. Cartoon representation of the GABA-AT dimer (pdb file 1ohv). Monomers are colored gray and light brown, respectively. PLP molecules are represented as green sticks. Mutation sites are indicated on the gray monomer and highlighted as magenta sticks. Images were rendered by PyMol software (Schrödinger, New York, NY, USA). (For interpretation of the references to colour in this figure legend, the reader is referred to the web version of this article.)

was found to be involved in the binding of the carboxylate group of the substrate [4]. As represented in **Fig. S1E**, the p.R220K substitution should have a minimal local structural impact, however, alterations of the catalytic activity of the enzyme are easily predictable, due to substrate binding alteration. Gln296 lies on the loop 292–306 of the large domain, behind the active site (**Fig. S1F**). Although the substitution p.Q296H is expected not to generate significant steric hindrance, it can abolish the polar contacts supported by the Gln side chain. Arg377 is located at the subunits interface and contributes to the monomer-monomer interaction (**Fig. S1G**). It is predictable that p.R377W substitution abolishes some interface contacts but, despite the large footprint of the Trp side chain, *in silico* mutagenesis suggests that the substitution should not generate massive steric hindrance. Gly465 is placed in the C-terminal domain in proximity to the active site. Both the substitution p.G465D and p.G465R generate substantial steric hindrance resulting in the possible repositioning of the proximal side chains (**Figs. S1H** and **S1I**). Both structural and catalytic effects are expected. Finally, Leu478 belongs to the loop 474–482 of the C-terminal domain and is involved in hydrophobic contacts (**Fig. S1L**). It is difficult to predict the overall structural effect of the introduction of a Pro residue in such position; indeed, the p.L478P substitution is expected to reduce the local flexibility of the backbone and limit the hydrophobic interactions.

3.2. Transfection of hGABA-AT wild-type in human cells and kinetic analysis

In order to identify a suitable human cell line exhibiting the lowest possible endogenous GABA-AT level, the level of expression of the endogenous enzyme was evaluated on five human cell lines (SH-SY5Y, HEK-293, HaCaT, HPDE-1, and fibroblasts). As expected, among the analyzed cells, the neuronal cell line (SH-SY5Y) displayed the highest level of endogenous GABA-AT (**Fig. S2A**). On the other hand, fibroblasts and HEK-293 exhibited the lowest GABA-AT expression level. With the aim to keep as low as possible the interference by the endogenous enzyme, both the latter cell lines were transfected with pGABA-AT expression plasmid and the levels of expression of the hGABA-AT protein were evaluated by western-blotting. Results show that, in comparison with the corresponding not transfected cells, the expression level of the protein was consistently higher in HEK-293 (Fig. 2) than in fibroblast (**Fig. S2B**). In fact, transfected HEK-293 cells exhibited at least 20 times increase of the hGABA-AT expression levels with respect to the not transfected cells; whereas, transfected fibroblasts displayed only a two-fold increase of the total GABA-AT protein (Fig. S2B), even with a higher amount of transfected DNA than HEK-293 cells. In addition, in fibroblasts no GABA transaminase enzymatic activity was detected on both transfected and not transfected cells (data not shown). Regarding HEK-293, the overexpressed protein displayed a single band with the same mobility of the endogenous enzyme and a molecular weight of around 50 kDa (Fig. 2A). This data suggests that, like the endogenous enzyme, the overexpressed hGABA-AT underwent the removal of the MTS signal peptide. To confirm this, confocal microscopy was used to verify the subcellular localization of the expressed hGABA-AT. As illustrated in Fig. 3A, while the control cells don't display detectable GABA-AT protein, in transfected cells hGABA-AT is clearly visible and colocalizes with mitochondria. These data were confirmed by the detection of expressed hGABA-AT in isolated mitochondria (Fig. 3B). In addition, unlike not-transfected cells, substantial GABA transaminase activity was detected in transfected HEK-293 cell lysate. Indeed, kinetic parameters of human GABA-AT were determined by analyzing the GABA transaminase activity on the soluble fraction of the cell lysate: K_M values of 2.2 ± 0.2 mM and 6.5 ± 0.7 mM were obtained for GABA and α-KG respectively, from the Michaelis curves reported in **Fig. S3**. From the mean of the V_{max} values a specific activity of 4×10^{-2} nmoles of SSA/min/μg of proteins was finally calculated. On the basis of all these results, we adopted the HEK-293 cells to express and analyze the wild type form and the pathogenic variants of hGABA-AT.

3.3. Expression and analysis of hGABA-AT pathogenic variants in HEK-293 cells

To acquire information about the structural and catalytic effects of the pathogenic amino acid substitutions on hGABA-AT, HEK-293 cells were transfected with the expression vectors of p.R92Q, p.P152S, p.L211F, p.F213C, p.R220K, p.Q296H, p.R377W, p.G465D, p.G465R, and

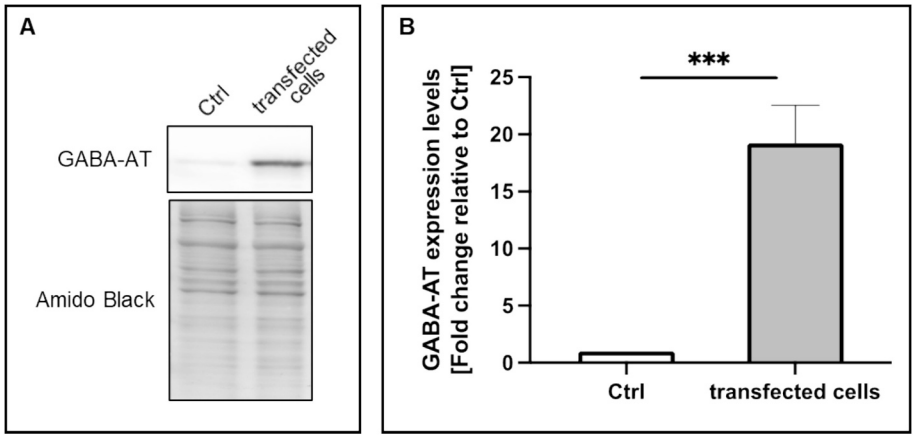

Fig. 2. Expression of hGABA-AT in HEK-293 cells. (**A**) Representative immunoblot of the expression of GABA-AT in control cells (Ctrl, *i.e.* not transfected cells) and in transfected cells with 1 μg of DNA expressing GABA-AT wild-type; (**B**) Densitometry analysis average of three different biological replicates. Amido Black is shown as loading control. Values are reported as fold change relative to Ctrl cells. Statistical legend: $p < 0.001$ (***).

p.L478P hGABA-AT variants. After 72 h, cells were collected, and the expression level (**Fig. S4**) and the specific activity of each mutant were evaluated on the soluble fraction of the cell lysate. The reported expression levels and the specific activity are the mean of independent experiments and are reported as fold change over the wild-type (Fig. 4**).** Even if to a different extent, all the variants exhibited a reduction of protein level and specific activity with respect to the hGABA-AT wild type. In particular, (i) p.P152S, p.L211F, and p.L478P variants are characterized by an undetectable residual specific activity and a low or modest enzyme expression level; (ii) p.R220K, p.Q296H, and p.R377W variants exhibit high expression level (81, 60, and 50 %, respectively, of that of WT) accompanied by a very low or undetectable specific activity; (iii) the p.R92Q, p.F213C, p.G465D, and p.G465R variants display 25–30 % of the expression level and a 10–16 % of the specific activity. On the basis of these results, it could be suggested that, while p.P152S, p.L211P, and p.L478P substitutions cause consistent alterations in both protein structure and catalysis, the p.R220K, p.Q296H, and p.R377W substitutions have a slight structural impact on the protein conformation but give rise to a strong reduction of the specific activity. Again, the p.R92Q, p.F213C, p.G465D, and p.G465R variants show an almost equal impact on both the expression level and the specific activity. The value of the specific activity (%)/expression level (%) ratio allowed us to estimate the relative specific activity (relative SA) of several variants, being a useful indicator to evaluate the actual effect of each mutation on the catalytic ability (Table 1). Among variants for which it is possible to measure the value of this ratio, it can be observed that the p.R220K displays a strong reduction of the catalysis (relative SA value equal to 5 %), while the p.R92Q, p.F213C, p.G465D, and p.G465R show a moderate reduction of the relative SA, ranging from 34 to 65 %.

4. Discussion

GABA transaminase deficiency is an autosomal recessive disorder caused by mutations in the *ABAT* gene, resulting in the accumulation of GABA in CSF. At present, little is known about the molecular defects of pathogenic hGABA-AT variants. The identification of the effect(s) of each single pathogenic variants at the protein level can help to better understand the molecular pathology of GABA-AT deficiency. Here, the pathogenic amino acid substitutions associated with GABA transaminase deficiency reported on HGMD database (*i.e.*, p.R92Q, p.P152S, p.L211F, p.R220K, p.Q296H, p.R377W, p.G465R, and p.L478P together with the more recently reported p.F213C and p.G465D [16]) have been biochemically characterized through the expression of hGABA-AT variants in a suitable cell line. Indeed, among different cell lines, HEK-293 cells have been selected as the best cellular models since it displayed (i) low expression level of the endogenous hGABA-AT with undetectable GABA transaminase activity, (ii) expression level of the exogenous hGABA-AT wild type protein at least 20 times higher than the not-transfected cells, and (iii) high GABA transaminase activity detectable on cells transfected with hGABA-AT expression plasmid. In addition, the mitochondrial localization of the overexpressed hGABA-AT was confirmed in these cells. These data suggested that the expressed protein is soluble, catalytically active, and follows the proper maturation pathway, undergoing the removal of the MTS signal peptide being correctly imported into the mitochondria. By means of the same expression system, the expression level and the specific activity of 10 pathogenic variants were analyzed and compared with those of hGABA-AT wild-type. In addition, *in silico* investigation on amino acids conservation, predicted ΔΔG values and possible local effects of the substitutions were used to support the biochemical data in the following discussion. On the basis of the soluble protein expression levels and transaminase activity, the analyzed variants can be divided into three group: (1) variants exhibiting strong impact on protein expression level together with no detectable catalytic activity (p.P152S, p.L211F, p.L478P); (2) variants characterized mainly by a strong catalytic defect (p.R220K, p.Q296H and p.R377W); and (3) variants exhibiting reduction on both protein expression and catalytic activity (p.R92Q, p.F213C, p.G465D and p.G465R).

The first group of variants includes p.P152S, p.L211F, and p.L478P and is characterized by structural defects, as suggested by the low protein expression level (5–36 %), and by undetectable GABA transaminase activity. About p.P152S and p.L478P, the introduction/removal of proline residues can potentially cause changes of the backbone flexibility. The marked structural instability of p.P152S variants was previously suggested also by MD simulation analysis [22]. Moreover, the very low expression levels of p.P152S and p.L478P makes it difficult to clarify whether p.P152S and p.L478P variants maintain residual catalytic activity. Similar results were found for p.L211F. Compared to the wild type hGABA-AT, p.L211F exhibits 36 % of protein expression level and undetectable catalytic activity. The effect of the p.L211F on the active site might be indirect, possibly transmitted through the loop 199–122, as for the p.F213C variant. A strong impact of these three substitutions on the protein stability is also supported by the high ΔΔG values predicted for these variants (red bars in **Fig. S5**).

The second group, *i.e.*, p.R220K, p.Q296H and p.R377W, can be considered mainly catalytic variants. The slight structural impact of these missense changes is confirmed by the predicted medium-low ΔΔG values (yellow bars in **Fig. S5**). In particular, Arg220 is a key active site residue directly involved in the binding of the GABA α-carboxylate group [3]. It is reasonable to suggest that the consistent loss of

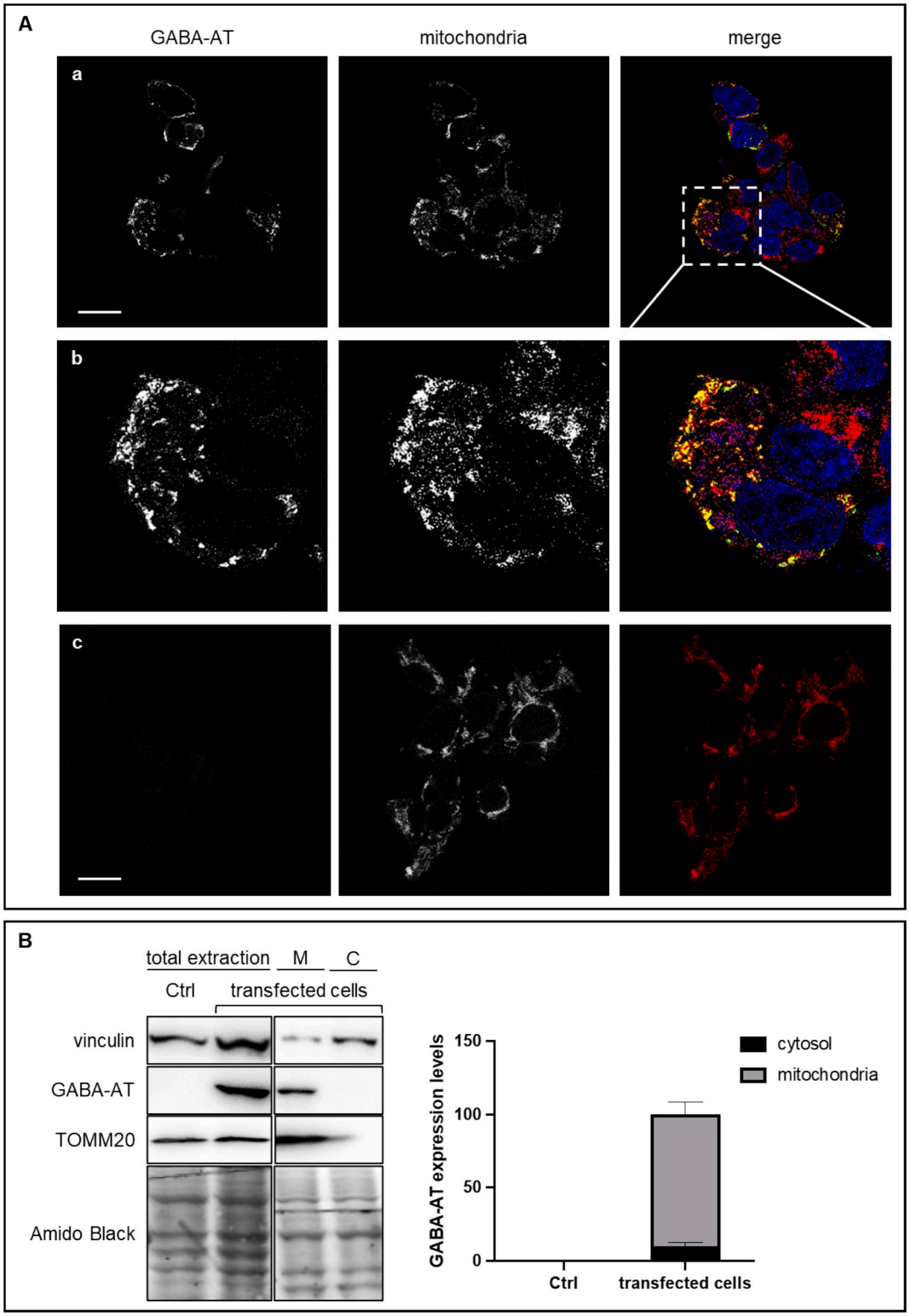

Fig. 3. Subcellular localization analyses. (**A**) Representative confocal images of GABA-AT (green signal) correctly localized in mitochondria stained with TOMM20 (red signal), and nucleus stained with DAPI (blue signal). The colocalization of GABA-AT and mitochondria is in light orange (panels a and b, which is a zoomed section). In panel C, control cells (*i.e.*, not transfected) are shown. Merged images come from a single z-plane; all the images were deconvolved. Images were captured at 63× magnification. Scale bar: 10 μm (a and c); panel b is an optic zoom of image A. (**B**) On the left, representative immunoblot of the different expression of vinculin, GABA-AT, and TOMM20 in mitochondria or cytosol in HEK-293 control cells (Ctrl, *i.e.*, not transfected cells) and in transfected cells with 1 μg of DNA expressing GABA-AT wild-type; on the right, densitometry analysis average of two different biological replicates. Amido Black is shown as loading control. (For interpretation of the references to colour in this figure legend, the reader is referred to the web version of this article.)

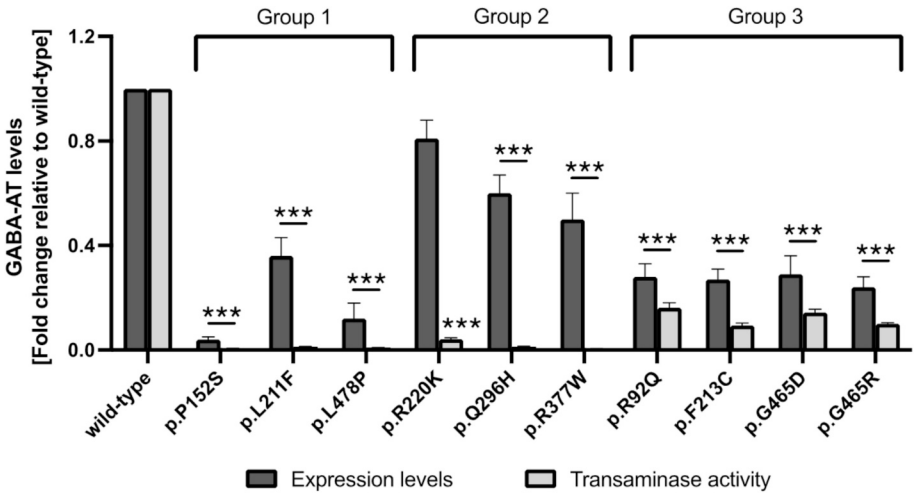

Fig. 4. Expression level and specific activity of the hGABA-AT pathogenic variants. The histogram represents the expression levels (dark gray) and specific activity (light gray) of GABA-AT. Specific GABA transaminase activity was measured in 50 mM Hepes pH 8.0, 150 mM NaCl, in the presence of 30 mM GABA, 50 mM α-KG, and 30 μM PLP. Values are reported as fold change relative to wild-type. The values are the means (± SE) of at least three independent biological replicates. Statistical legend: $p < 0.001$ (***) *versus* wild-type. Groups 1, 2, and 3 are indicated according to the classification described in the discussion.

Table 1
Specific activity and expression levels of the hGABA-AT variants expressed in HEK-293 cells. Expression level and specific activity (SA) were calculated on HEK-293 soluble lysate as percentage of the wild-type hGABA-AT expression and GABA transaminase activity. Relative SA of each variant was calculated as (SA /Expression level) x100.

Enzymatic species	Expression level (%)	SA (%)	Relative SA (%)
R92Q	25 ± 4	16.2 ± 1,1	65 ± 13
P152S	4 ± 1	n.d.	n.d.
L211F	36 ± 7	n.d.	n.d.
F213C	27 ± 4	9.3 ± 0.9	34 ± 8
R220K	81 ± 7	4.2 ± 0.5	5 ± 1
Q296H	60 ± 6,5	n.d.	n.d.
R377W	50 ± 10	n.d.	n.d.
G465D	29 ± 5,3	14.4 ± 1.2	50 ± 13
G465R	24 ± 4.1	10.1 ± 0.3	42 ± 8
L478P	12 ± 6,4	n.d.	n.d.

transaminase activity of p.R220K substitution can be due to a dramatic reduction of substrate binding affinity and/or specificity. The same biochemical profile was reported for the pathogenic substitution of the corresponding residue (Arg180) of human ornithine aminotransferase [23]. A similar behavior was observed here for the p.Q296H variants. The proximity of Gln296 to the PLP binding pocket makes it possible to suggest an indirect effect of the substitution p.Q296H on the active site. Nevertheless, in-depth structural analysis would be needed to better explain the absence of detectable catalytic activity of this variant. Moreover, the rather high level of soluble p.Q296H protein indicates that this mutation seems to not have a significant impact on the folding or solubility of the enzyme. The p.R377W variant displayed a consistent protein level but not detectable SA. From the *in silico* inspection, p. R377W resulted an interface mutation because Arg377 is involved in the monomer-monomer interaction of hGABA-AT (see above). Several reported evidences indicated that mutations at the dimer interface of Fold Type I PLP-dependent enzymes have an impact on the catalytic activity [24]. That is not surprising considering that, in this class of proteins, active sites are located at the monomer interface and are composed of residues belonging to both subunits [25]. Therefore, despite the drastic amino acid substitution, p.R377W was mainly characterized by a catalytic defect.

The third group of variants comprises p.R92Q, p.F213C, p.G465D, and p.G465R. These displayed 25–50 % of the soluble protein level and maintained about one half (42–64 %) of relative SA. The p.R92Q exhibited only 25 % of protein level. This is in line with the reported MD simulation analysis suggesting the p.R92Q instability [22]. On the other hand, the p.R92Q variant showed 65 % residual SA, the highest among the analyzed variants. This finding indicates that p.R92Q has mainly a structural impact with moderate effect on catalytic ability. This is in line with the peripheral surface location of Arg92. Differently, p.F213C, p. G465D, and p.G465R variants showed almost equal soluble protein levels and relative SA percentages. Based on *in silico* mutagenesis, the loss of apolar contacts and the impact on the loop 199–122 are possible structural effects of the p.F213C, as well as both the p.G465D and p. G465R are predicted to perturb the local microenvironment in the proximity of the active site.

On the basis of the presented classification, variants belonging to the first and second group exhibit stronger defects with respect to those of the third group. In fact, variants belonging to the first group are characterized by a consistent structural impact indicated by a very low expression level and high ΔΔG values, while those of the second group present a remarkable catalytic defect. Finally, the variants of the third group, despite a significant reduction of the protein level, maintain a substantial GABA transaminase activity, suggesting the presence of a higher amount of functional protein with respect to the other two groups of variants.

5. Conclusions

Human GABA transaminase is a key enzyme in the GABA metabolism. Pathogenic mutations of the *ABAT* gene cause GABA-AT deficiency, an ultra-rare autosomal recessive disorder. In this work, 10 pathogenic variants of the hGABA-AT associated with GABA transaminase deficiency have been characterized through expression in HEK-293 cells and bioinformatic analysis. Protein expression level, GABA transaminase activity, *in silico* mutagenesis, and ΔΔG prediction allowed us to classify the variants into 3 groups: 1) variants with strong structural defects associated with undetectable catalytic activity (p.P152S, p. L211F and p.L478P); 2) variants characterized mainly by a catalytic defect (p.R220K, p.Q296H and p.R377W); 3) variants exhibiting both structural and catalytic defect maintaining substantial catalytic activity (p.R92Q, p.F213C, p.G465D and p.G465R); On the basis of these findings the strongest defects were attributed to the variants belonging to the first and second group. Patients affected by GABA transaminase deficiency display a broad phenotypic spectrum [13,15]. To improve the understanding of genotype-phenotype relationships and gain insight

into the molecular pathogenesis of GABA-AT deficiency, a deeper knowledge of the molecular effects caused by each mutation on the GABA-AT protein is needed. In this study, for the first time, we associated 10 pathogenic variants of hGABA-AT with specific molecular defects. In conclusion, our results open the way to the characterization of the different enzymatic phenotypes responsible for the broad clinical spectrum and variable response to treatments in GABA-AT deficiency.

CRediT authorship contribution statement

Giulia Ambrosini: Writing – review & editing, Investigation, Formal analysis. **Fulvio Floriani:** Methodology, Investigation, Formal analysis. **Vittoria Manni:** Methodology, Investigation. **Ilaria Dando:** Writing – review & editing, Resources. **Riccardo Montioli:** Writing – review & editing, Writing – original draft, Supervision, Project administration, Conceptualization.

Funding

This research did not receive any specific grant from funding agencies in the public, commercial, or not-for-profit sectors.

Declaration of competing interest

The authors declare no competing financial interests.

Appendix A. Supplementary data

Supplementary data to this article can be found online at https://doi.org/10.1016/j.ymgme.2025.109149.

Data availability

Data will be made available on request.

References

[1] P.K. Mehta, T.I. Hale, P. Christen, Aminotransferases: demonstration of homology and division into evolutionary subgroups, Eur. J. Biochem. 214 (1993) 549–561.
[2] A. Besse, P. Wu, F. Bruni, T. Donti, B.H. Graham, W.J. Craigen, R. McFarland, P. Moretti, S. Lalani, K.L. Scott, R.W. Taylor, P.E. Bonnen, The GABA transaminase, ABAT, is essential for mitochondrial nucleoside metabolism, Cell Metab. 21 (2015) 417–427.
[3] P. Storici, G. Capitani, D. De Biase, M. Moser, R.A. John, J.N. Jansonius, T. Schirmer, Crystal structure of GABA-aminotransferase, a target for antiepileptic drug therapy, Biochemistry 38 (1999) 8628–8634.
[4] P. Storici, D. De Biase, F. Bossa, S. Bruno, A. Mozzarelli, C. Peneff, R.B. Silverman, T. Schirmer, Structures of gamma-aminobutyric acid (GABA) aminotransferase, a pyridoxal 5′-phosphate, and [2Fe-2S] cluster-containing enzyme, complexed with gamma-ethynyl-GABA and with the antiepilepsy drug vigabatrin, J. Biol. Chem. 279 (2004) 363–373.
[5] K. Gale, GABA in epilepsy: the pharmacologic basis, Epilepsia 30 (Suppl. 3) (1989) S1–11.
[6] J.Y. Wu, E.D. Bird, M.S. Chen, W.M. Huang, Abnormalities of neurotransmitter enzymes in Huntington's chorea, Neurochem. Res. 4 (1979) 575–586.
[7] S. Grover, R.K. Narang, S. Singh, GABA-transaminase: a key player and potential therapeutic target for neurological disorders cent Nerv Syst agents, Med. Chem. 24 (2024) 57–67.
[8] B. Alharbi, H.M. Al-Kuraishy, A.I. Al-Gareeb, E. Elekhnawy, H. Alharbi, A. Alexiou, M. Papadakis, G.E. Batiha, Role of GABA pathway in motor and non-motor symptoms in Parkinson's disease: a bidirectional circuit, Eur. J. Med. Res. 29 (2024) 205.
[9] H.H.C. Lee, G.E. McGinty, P.L. Pearl, A. Rotenberg, Understanding the molecular mechanisms of succinic Semialdehyde dehydrogenase deficiency (SSADHD): towards the development of SSADH-targeted medicine, Int. J. Mol. Sci. 23 (2022).
[10] J. Jaeken, P. Casaer, P. de Cock, L. Corbeel, R. Eeckels, E. Eggermont, P. J. Schechter, J.M. Brucher, Gamma-aminobutyric acid-transaminase deficiency: a newly recognized inborn error of neurotransmitter metabolism, Neuropediatrics 15 (1984) 165–169.
[11] L.K. Medina-Kauwe, W.L. Nyhan, K.M. Gibson, A.J. Tobin, Identification of a familial mutation associated with GABA-transaminase deficiency disease, Neurobiol. Dis. 5 (1998) 89–96.
[12] M. Tsuji, N. Aida, T. Obata, M. Tomiyasu, N. Furuya, K. Kurosawa, A. Errami, K. M. Gibson, G.S. Salomons, C. Jakobs, H. Osaka, A new case of GABA transaminase deficiency facilitated by proton MR spectroscopy, J. Inherit. Metab. Dis. 33 (2010) 85–90.
[13] A. Besse, A.K. Petersen, J.V. Hunter, V. Appadurai, S.R. Lalani, P.E. Bonnen, Personalized medicine approach confirms a milder case of ABAT deficiency, Mol. Brain 9 (2016) 93.
[14] P. Louro, L. Ramos, C. Robalo, C. Cancelinha, A. Dinis, R. Veiga, R. Pina, O. Rebelo, A. Pop, L. Diogo, G.S. Salomons, P. Garcia, Phenotyping GABA transaminase deficiency: a case description and literature review, J. Inherit. Metab. Dis. 39 (2016) 743–747.
[15] M.K. Koenig, R. Hodgeman, J.J. Riviello, W. Chung, J. Bain, C.A. Chiriboga, K. Ichikawa, H. Osaka, M. Tsuji, K.M. Gibson, P.E. Bonnen, P.L. Pearl, Phenotype of GABA-transaminase deficiency, Neurology 88 (2017) 1919–1924.
[16] A.D. Kennedy, K.L. Pappan, T. Donti, M.R. Delgado, M. Shinawi, T.S. Pearson, S. R. Lalani, W.E. Craigen, V.R. Sutton, A.M. Evans, Q. Sun, L.T. Emrick, S.H. Elsea, 2-Pyrrolidinone and Succinimide as clinical screening biomarkers for GABA-transaminase deficiency: anti-seizure medications impact accurate diagnosis, Front. Neurosci. 13 (2019) 394.
[17] C. Jakobs, J. Jaeken, K.M. Gibson, Inherited disorders of GABA metabolism, J. Inherit. Metab. Dis. 16 (1993) 704–715.
[18] D.E. Pires, D.B. Ascher, T.L., Blundell, mCSM: predicting the effects of mutations in proteins using graph-based signatures, Bioinformatics 30 (2014) 335–342.
[19] D.E. Pires, D.B. Ascher, T.L. Blundell, DUET: a server for predicting effects of mutations on protein stability using an integrated computational approach, Nucleic Acids Res. 42 (2014) W314–W319.
[20] C.H.M. Rodrigues, D.E.V. Pires, D.B. Ascher, DynaMut2: assessing changes in stability and flexibility upon single and multiple point missense mutations, Protein Sci. 30 (2021) 60–69.
[21] C. Lu, C. Wu, D. Ghoreishi, W. Chen, L. Wang, W. Damm, G.A. Ross, M.K. Dahlgren, E. Russell, C.D. Von Bargen, R. Abel, R.A. Friesner, E.D. Harder, OPLS4: improving force field accuracy on challenging regimes of chemical space, J. Chem. Theory Comput. 17 (2021) 4291–4300.
[22] M. Yasir, J. Park, E.T. Han, W.S. Park, J.H. Han, Y.S. Kwon, H.J. Lee, W. Chun, Computational exploration of the effects of mutations on GABA aminotransferase in GABA aminotransferase deficiency, Int. J. Mol. Sci. 24 (2023).
[23] R. Montioli, A. Paiardini, G. Giardina, S. Zanzoni, F. Cutruzzola, B. Cellini, C. Borri Voltattorni, R180T variant of delta-ornithine aminotransferase associated with gyrate atrophy: biochemical, computational, X-ray and NMR studies provide insight into its catalytic features, FEBS J. 286 (2019) 2787–2798.
[24] F. Floriani, C. Borri Voltattorni, B. Cellini, R. Montioli, Biochemical and Bioinformatic studies of mutations of residues at the monomer-monomer Interface of human ornithine aminotransferase leading to gyrate atrophy of choroid and retina, Int. J. Mol. Sci. 24 (2023).
[25] A.C. Eliot, J.F. Kirsch, Pyridoxal phosphate enzymes: mechanistic, structural, and evolutionary considerations, Annu. Rev. Biochem. 73 (2004) 383–415.